

Micro-explosive-induced underwater shock wave propagation and reflection at the interface

Kiyonobu Ohtani*[†] and Toshihiro Ogawa*

*Institute of Fluid Science, Tohoku University,
2-1-1, Katahira, Aoba, Sendai 980-8577, JAPAN
Phone : +81-22-217-5037

[†]Corresponding author : ohtani@ifs.tohoku.ac.jp

Received : November 14, 2014 Accepted : July 3, 2015

Abstract

This paper reports the results of experiments on underwater shock wave propagation and reflection at the interface of certain materials conducted to improve the understanding of shock wave interaction with the interface of materials with different acoustic impedance. An underwater shock wave was generated by detonating a micro-explosive (AgN_3) near the interface of materials with different acoustic impedance (water and acrylic/aluminum/stainless steel/air). The process of shock wave propagation was visualized by the shadowgraph method and recorded by an ultra-high-speed camera. The pressure history near the interface was measured simultaneously by a needle hydrophone with high spatiotemporal resolution. Time-resolved shadowgraph images show that a compression wave was reflected from a thin interface plate, and an expansion wave, which propagated downward, was then generated in water by reflection from the air. In addition, a cavitation bubble was created behind the expansion wave. The simultaneously measured pressure history also shows that an expansion wave propagated behind the compression wave.

Keywords : shock wave, expansion wave, micro-explosive, acoustic impedance, shadowgraph, pressure history

1. Introduction

Underwater shock waves and expansion waves and their induced phenomena, such as production of cavitation bubbles associated with human tissue damage by shock waves, are an important area of research for shock wave medical and biomedical application^{1)–4)}. Tissue damage is an important issue for shock wave medical application and is caused by shock wave and expansion wave phenomena.

It should be specially noted that an expansion wave is generated by an underwater shock wave reflecting from the water surface, a medium with lower acoustic impedance^{5)–8)}. Acoustic impedance z is defined as $z = \rho c$, where ρ is the density of the material, c is the speed of sound. A shock wave is transmitted directly at an interface of two materials with the same acoustic impedance. In the case of reflection at an interface with a material with higher acoustic impedance, a shock wave is transmitted only partially and is reflected mostly as a compression wave. On the other hand, in the case of reflection at an interface with a material with lower acoustic impedance, a shock wave is transmitted only

partially, and the remaining wave is reflected as an expansion wave. Additionally, the reflection coefficient R_p is determined by the following Equation (1),

$$R_p = \frac{P_r}{P_i} = \frac{Z_2 - Z_1}{Z_2 + Z_1} \quad (1)$$

where P_i and P_r are, respectively, the incident and reflected shock peak pressure, Z_1 and Z_2 are the acoustic impedance of the material on the incident and transmission sides, respectively.

The human body is composed of various organs and tissues with different acoustic impedance. During shock wave propagation in human tissues, the interaction phenomena are very complex because of the acoustic impedance mismatch at the interfaces. Therefore, the shock wave interaction phenomena at the interface of materials with different acoustic impedance have to be evaluated to improve understanding of the mechanism of shock wave tissue damage. However, the effect of acoustic impedance on these phenomena is still poorly understood.

In the present study, as the initial step for this goal, an

experiment on propagation of micro-explosive-induced underwater shock wave and their reflection at the interface of materials with different acoustic impedance was performed for a quantitative evaluation. The process of micro-explosive-induced underwater shock wave propagation and reflection at the interface was visualized by the shadowgraph method and recorded by an ultra-high-speed camera at high spatiotemporal resolution. The shock wave pressure history near the interface was measured simultaneously by a needle hydrophone with high spatiotemporal resolution.

2. Experimental setup

Figure 1 shows the experimental setup for observation of underwater shock wave propagation and reflection at the interface in a stainless water-filled chamber. The water chamber with dimensions of $200 \times 200 \times 200$ [mm] was used, which was equipped with a 200×200 [mm] acrylic observation window. An underwater shock wave was generated by detonating a micro-explosive (silver azide, AgN_3 , Showa Kinzoku Kogyo Co., Ltd., density of 3.8 [g cm^{-3}], weight of 10 ± 0.1 [mg], diameter of 1.5 [mm], length of 1.5 [mm]). The silver azide pellet is glued at the tip of a quartz optical fiber (G.C. 600/750, Fujikura Ltd.) and placed at a distance of about 20.0 [mm] from the impedance interface (water surface or other material's surface in water, that is the interface of water and a thin plate). In this study, thin plates made of acrylic, aluminum (AL5052), stainless steel (SUS304) (100×100 [mm], thickness of 1 [mm]) were used as the interface with water. The experimental conditions of this study are shown in Table 1. A Q-switched pulsed Nd: YAG laser beam (SAGA220, B.M. Industries, 7 [ns] pulse duration, about 25 [mJ] per pulse) was guided through the optical fiber and then ignited the micro-explosive.

Table 2 shows the list of acoustic impedance values for air, water, conventional solid materials used in this study, and human tissues^{3), 9)–12)}. The acoustic impedance of

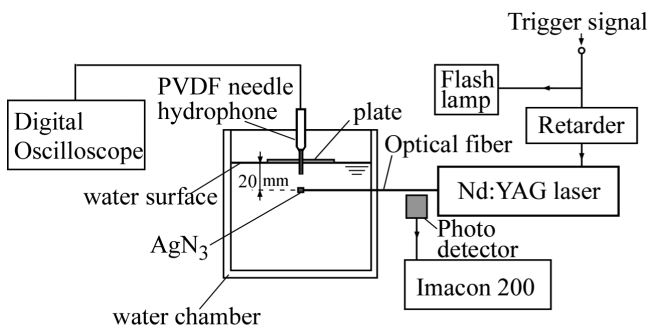


Figure 1 Schematic diagram of the experimental setup for observation of underwater shock wave reflection and transmission at the interface.

Table 1 Experimental conditions of the interface materials.

Test number	1st layer	2nd layer	3rd layer
#1	water	air	–
#2	water	acrylic	air
#3	water	aluminum	air
#4	water	stainless steel	air

Table 2 List of acoustic impedance values of air, water, some conventional solid materials, and tissues.

Material	Density ρ [kg m^{-3}]	Sound speed c [m s^{-1}]	Acoustic impedance $Z = \rho c$ [$\text{kg m}^{-2} \text{s}^{-1}$]
1 Air ⁹⁾	1.2929	331.45	428.6
2 Water (23–27° C) ⁹⁾	1.0×10^3	1500	1.50×10^6
3 Acrylic ¹⁰⁾	1.182×10^3	2600	3.07×10^6
4 Aluminum 5052 ¹¹⁾	2.68×10^3	6142	16.5×10^6
5 Stainless Steel 304 ¹²⁾	7.90×10^3	4570	36.1×10^6
6 Blood ³⁾	–	–	1.61×10^6
7 Brain ³⁾	–	–	1.58×10^6
8 Lung ³⁾	–	–	0.26×10^6
9 Bone ³⁾	–	–	$2.1 - 7.8 \times 10^6$

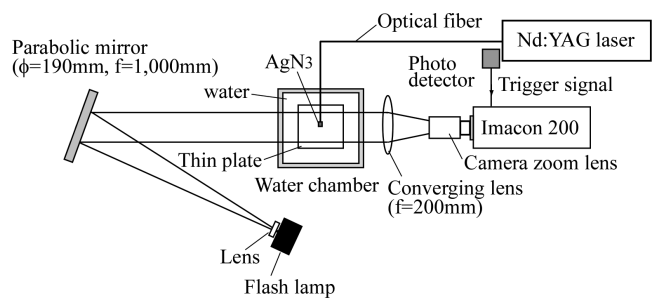


Figure 2 Schematic diagram of optical setup for the shadowgraph method.

human tissue is less than about 8.0×10^6 [$\text{kg m}^{-2} \text{s}^{-1}$]³⁾. Therefore, the materials used in this study are sufficient for simulation of a biomedical material.

Figure 2 shows the schematic of the optical setup for the shadowgraph method, which used a parabolic mirror (focal length of $1,000$ [mm], diameter of 190 [mm]). A flash lamp (PE-5651, Panasonic Inc.) was used as the light source and was triggered via a digital retarder (RE-306, Sugawara Laboratories Inc.) synchronizing with an ultra-high-speed framing camera. The process of shock wave propagation and the reflection phenomena at the interface were visualized by this shadowgraph optical setup and recorded by the ultra-high-speed framing camera (Imacon 200, DRS Technologies, Inc., resolution of 1200×980 pixel per frame, framing rates up to 200 Mfps, exposure time of 5 [ns] to 2 [ms]). A converging lens and a camera zoom lens (Model A20, $f = 28\text{--}300$ [mm], Tamron) was used to focus on the region near the interface of water with air or a thin plate. The pressure history in water near the interface was measured simultaneously by a spatiotemporal PVDF (polyvinylidene difluoride) needle hydrophone (Platte Needle Probe, Müller Instruments, detectable pressure range of -10 to 200 [MPa], sensitive diameter of 0.5 [mm], rise time of 50 [ns]) and recorded by a digital oscilloscope (DL7500, 10 MS/s, Yokogawa).

3. Results and discussion

Figure 3 shows sequential shadowgraph images of micro-explosive-induced underwater shock wave propagation and reflection at the interface. The

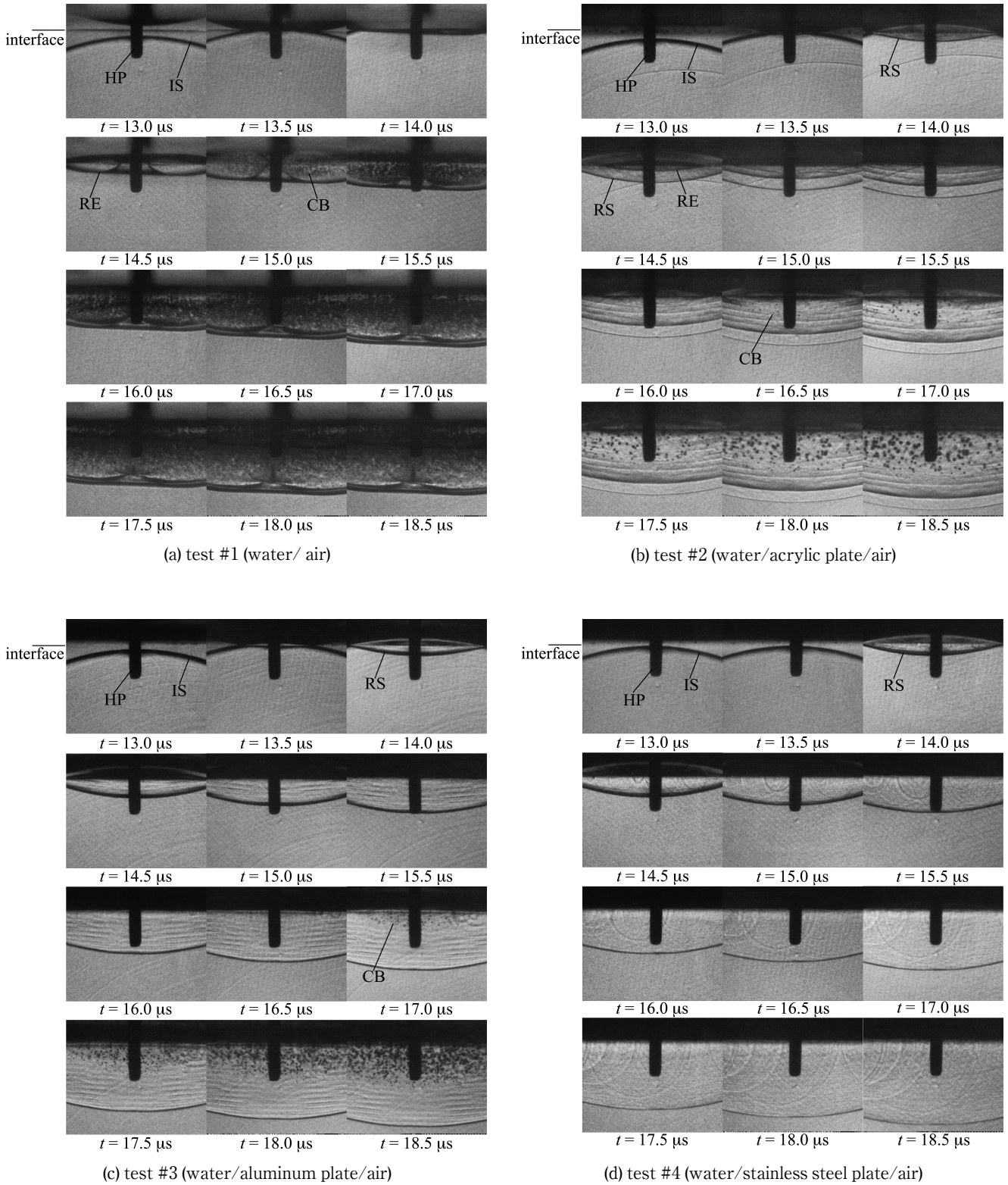


Figure 3 Sequential shadowgraph images of underwater shock wave reflection and transmission at the interface. (Inter-frame time 500 [ns], exposure time 10 [ns]) IS: Incident Shock Wave, RS: Reflected Shock Wave, RE: Reflected Expansion Wave, CB: Cavitation Bubble, HP: Hydrophone)

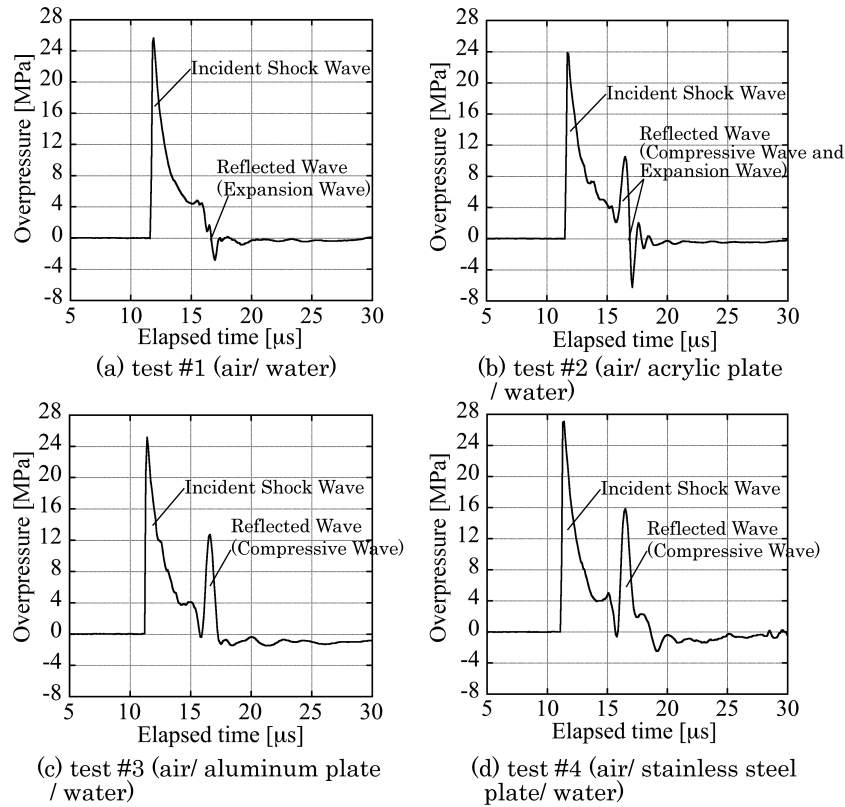


Figure 4 Pressure histories near the interface.

observation was performed at the visualization region of about 13.5×11.0 [mm], the inter-frame time of 500 [ns] (2 Mfps) and the exposure time of 10 [ns], which was enough to capture the underwater shock wave front without blurring.

The case of water-air interface (test #1) is shown in Figure 3(a). At 13.0 [μ s] after ignition of the micro explosive, the induced underwater shock wave almost reached the interface. The shock wave was reflected from the interface of water and air as an expansion wave. The pressure near the water surface was decreased by propagation of the expansion wave, and a cavitation bubble was created behind the expansion wave.

The case of water, thin acrylic plate and air interface (test #2) is shown in Figure 3(b). The underwater shock wave was reflected at the interface, along with multiple other waves. The first reflected wave is a compressive wave. However, the secondary wave is an expansion wave, because a cavitation bubble is created behind this wave. The first wave is reflected from the thin acrylic plate, and the secondary wave is the reflected expansion wave from the interface of the acrylic plate and air. This expansion wave and the subsequent waves were generated by the transmitted compressive wave propagating and reflecting repeatedly in the thin acrylic plate. The reflected wave from the thin acrylic plate with the relatively low acoustic impedance is a clear combination of a compressive wave and an expansion wave. The interval between the first and second reflected wave fronts measured by the sequential images was about 1.09 mm, equal to the propagation distance in water over the time required for propagating across the thin plate at the sound speed of acrylic.

Table 3 Reflection coefficients.

Test number	R_{p-exp}	R_{p-theo}
#2	0.41	0.34
#3	0.51	0.83
#4	0.55	0.92

The case of water, thin aluminum plate and air interface (test #3) is shown in Figure 3(c). Aluminum has higher acoustic impedance than acrylic. The underwater shock wave was reflected at the interface, followed by multiple other reflected waves. The first reflected wave was a compressive wave in the same way as in test #2. However, the secondary and subsequent reflected waves of unclear nature were also propagating downward. The gap between the first and second reflected wave front is shorter than that in the case of test #2. In this case, the shock wave reflects from the thin aluminum plate as a mostly compressive wave. Although only a small part of the transmitted compressive wave is reflected as an expansion wave, a cavitation bubble is generated.

The case of water, a thin stainless steel plate and air interface (test #4) is shown in Figure 3(d). Stainless steel has higher acoustic impedance than acrylic and aluminum. The underwater shock wave was reflected at the interface, a compressive wave propagated downward, and then an unclear expansion wave and subsequent waves with shorter intervals were generated, but a cavitation bubble near the interface did not occur. In other words, most of the incident shock wave was reflected as a compressive wave, and only a small part is transmitted into the stainless steel plate. As a result, the reflected expansion wave was weaker.

Figure 4 shows the measured pressure histories near the interface in water at a distance of about 3 [mm] from the interface. In all interface cases, at about 12 [μ s], the incident shock wave reached the tip of the needle hydrophone, after which the pressure raised sharply and reduced immediately. Further, at about 16 [μ s], the reflected wave was detected. In the interface case of water and air (test #1), as shown in Figure 4(a), when the reflected wave, that is, the expansion wave, arrived, the pressure decreased to about -2.8 [MPa]. However, in the interface case of water, thin acrylic plate and air (test #2), as shown in Figure 4(b), two reflected waves with relatively high amplitude arrived as a compressive and expansion waves as identified above. The negative peak pressure of the expansion wave reached -6.3 [MPa], which is lower than the interface case of water and air (test #1). The larger the difference in acoustic impedance between the propagation medium and air is, the smaller the negative peak pressure becomes. In the interface case of water, thin aluminum plate and air (test #3), as shown in Figure 4(c), the peak overpressure of the reflected compressive wave was higher than the interface case of water, thin acrylic plate and air (test #2). In this case, the expansion wave behind the reflected compressive wave was unclear, and the pressure amplitude was lower than for the interface of water, thin acrylic plate and air (test #2). In the interface case of water, thin metallic plate and air (test #3 and #4), the peak overpressure of the reflected shock wave was higher than in the interface case of water, thin acrylic plate and air (test #2). Thus, the larger the difference in acoustic impedance between the reflective medium and water becomes, the larger the peak overpressure of the reflected compressive wave becomes.

This behavior was substantiated acoustically, that is, the reflection coefficient R_p , as indicated by Equation (1). Table 3 shows the reflection coefficient R_p calculated by using Equation (1) from the measured shock peak overpressure data and acoustic impedance values (Table 2). The reflection coefficient calculated from the experimental results R_{p-exp} increased with the growing difference in acoustic impedance of the interface, as indicated by the acoustic theory. However, R_{p-exp} is small in comparison with the theoretically calculated reflection coefficient R_{p-theo} , particularly in the case of the large difference in acoustic impedance (test #3 and #4). Because the high peak overpressure of a shock wave attenuates rapidly, the measured peak overpressure of the reflected shock wave was already damped in this case. Therefore, experiments for a detailed understanding of this behavior need to measure the peak overpressure at various positions.

4. Conclusion

In this study, highly spatiotemporal observations were performed to understand the effect of acoustic impedance on shock wave interaction phenomena. A series of cases of shock wave propagation and reflection at the interface of

materials with different acoustic impedance at 2 Mfpa were visualized by the shadowgraph method, and shock wave pressure history near the interface was measured simultaneously by a needle hydrophone with high spatiotemporal resolution.

An expansion wave was generated by the transmitted shock wave reflecting from the interface of a thin plate (acrylic or aluminum) and air, with a cavitation bubble subsequently occurring near the interface. The negative peak pressure of the expansion wave in the case of water, acrylic plate and air interface was lower than in the case of water and air, because of the large difference in acoustic impedance between the propagation medium and air. The reflection coefficient calculated from the experimental results increased with growing difference in acoustic impedance of the interface, as indicated by the acoustic theory.

The present paper reports a qualitative evaluation of shock wave interaction phenomena at the interface of materials with different acoustic impedance. A quantitative evaluation of these phenomena needs more detailed data regarding plate thickness, incident shock wave pressure, interface material, and will be reported in our subsequent paper. This study has the potential to be utilized in the methods of protection from shock wave tissue damage.

Acknowledgement

This work was supported by a MEXT KAKENHI Grant No. 26420100, by a Foundation for the Promotion of the Industrial Explosives Technology in 2014.

References

- 1) M. Delius, Shock Waves, 4, 55 – 72 (1994).
- 2) M. Delius, K. Draenert, Y. Draenert and M. Börner, "Extracorporeal Shock Waves in Orthopedics", 91 – 107, Berlin : Springer-Verlag (1998).
- 3) A. Nakagawa, G.T. Manley, A.D. Gean, K. Ohtani, R. Armonda, A. Tsukamoto, H. Yamamoto, K. Takayama and T. Tominaga, J. Neurotrauma, 28, 1101 – 1119 (2011).
- 4) K. Takayama and T. Saito, Annu. Rev. Fluid Mech., 36, 347 – 379 (2004).
- 5) V.K. Kedrinskii, J. Appl. Mech. And Tech. Phys., 16(5), 724 – 733 (1975).
- 6) V.K. Kedrinskii, Acta Astronautica, 3, 623 – 632 (1976).
- 7) K. Ohtani, T. Hashimoto and K. Takayama, Proc. 27th Int. Symp. Shock Waves, 297, St. Petersburg, Russia (2009).
- 8) K. Ohtani, T. Ogawa and S. Obayashi, Proc. 8th Int. Conf. Flow Dynamics, 134 – 135, Sendai, Japan (2011).
- 9) National Astronomical Observatory of Japan (ed.): "Chronological Scientific Tables", Maruzen, Tokyo, (2015). (in Japanese).
- 10) J.P. Borg, L. Schwalbe, J. Cogar, D.J. Chapman, K. Tsembeles, A. Ward and A. Lloyd, AIP Conf. Proc., 845, 37 (2006).
- 11) P.E. Specht, PhD Thesis, Georgia Institute of Technology, (2013).
- 12) D.J. Steinberg, Lawrence Livermore National Laboratory Report. UCRL-MA-106439 (1996).